Journal of Power Sources 256 (2014) 329–335

Contents lists available at ScienceDirect

Journal of Power Sources

journal homepage: www.elsevier.com/locate/jpowsour

Three dimensional graphene foam supported platinum–ruthenium bimetallic nanocatalysts for direct methanol and direct ethanol fuel cell applications

Chih-Chien Kung [a,*], Po-Yuan Lin [b], Yuhua Xue [c], Rohan Akolkar [a], Liming Dai [c], Xiong Yu [d], Chung-Chiun Liu [a]

[a] Department of Chemical Engineering, Case Western Reserve University, 10900 Euclid Avenue, Cleveland, OH 44106, USA
[b] Department of Materials Science and Engineering, Case Western Reserve University, Cleveland, OH 44106, USA
[c] Department of Macromolecular Science and Engineering, Case Western Reserve University, Cleveland, OH 44106, USA
[d] Department of Civil Engineering, Case Western Reserve University, Cleveland, OH 44106, USA

HIGHLIGHTS

- 3D graphene foam was used as the scaffold for the deposition of PtRu nanoparticles.
- PtRu/3D graphene foam nanocatalyst showed excellent catalytic activity performance.
- PtRu/3D graphene foam nanocatalyst exhibited a higher tolerance to poisoning CO.

ARTICLE INFO

Article history:
Received 11 October 2013
Received in revised form
13 January 2014
Accepted 17 January 2014
Available online 25 January 2014

Keywords:
PtRu bimetallic nanoparticles
Nanocatalysts
Carbon supporting materials
Methanol oxidation reaction
Ethanol oxidation reaction
Three-dimensional graphene foam

ABSTRACT

A novel composite material of hierarchically structured platinum–ruthenium (PtRu) nanoparticles grown on large surface area three dimensional graphene foam (3D GF) is reported. 3D GF was incorporated with PtRu bimetallic nanoparticles as an electrochemical nanocatalyst for methanol and ethanol oxidation. PtRu/3D GF nanocatalyst showed a higher tolerance to poisoning by CO and exhibited improved catalytic activity for both methanol oxidation reaction (MOR) and ethanol oxidation reaction (EOR). Cyclic voltammetry (CV) results and long-term cycling stability tests demonstrated that GF provided a promising platform for the development of electrochemical nanocatalysts. Specifically, PtRu/3D GF nanocatalyst showed excellent catalytic activity toward MOR and EOR compared with PtRu/Graphene (Commercial graphene), PtRu/C (Vulcan XC-72R carbon), and PtRu alone. The crystal size of PtRu on 3D GF was reduced to 3.5 nm and its active surface area was enhanced to 186.2 $m^2\ g^{-1}$. Consequently, the MOR and EOR rates were nearly doubled on PtRu/3D GF compared to those on PtRu/Graphene.

1. Introduction

Fuel cells are an enabling technology for creating high performance energy conversion and storage devices [1,2]. Among different types of direct alcohol fuel cells (DAFCs), direct methanol fuel cells (DMFCs) and direct ethanol fuel cells (DEFCs) are excellent power sources due to their high energy density, low pollutant emission, low operating temperature, and easy fuel feeding [3,4].

Transition metal nanoparticles are used in the development of DAFCs due to their catalytic activity [5]. The large surface-to-volume ratio and special binding on the surface of nanoparticles leads to catalytic activity [6]. As an example, platinum (Pt) nanoparticles are used in DMFCs and DEFCs based on their catalytic activity for the oxidation of methanol and ethanol [4]. Electrodes modified with Pt nanoparticles enhance electron transfer and reduce the activation overpotential for methanol and ethanol oxidation [7]. Bimetallic nanoparticles create functional hybrid nanostructures, resulting in unique electronic, catalytic, or photonic properties. The addition of a second metal contributes to the alterations in particle size, shape, surface-morphology, composition, chemical and physical properties including the catalytic activity and chemical selectivity as compared to the single-metal nanocatalysts [8]. The low-loading and high catalytic activity of Pt-based nanocatalysts, which are essential for DMFC and DEFC

* Corresponding author. Tel.: +1 440 317 2816; fax: +1 216 368 8738.
E-mail address: cxk215@case.edu (C.-C. Kung).

0378-7753/$ – see front matter © 2014 Elsevier B.V. All rights reserved.
http://dx.doi.org/10.1016/j.jpowsour.2014.01.074

development, can be achieved by decreasing particle size, increasing number of active sites for methanol or ethanol, and increasing the resistance against CO poisoning [9]. Specifically, among platinum based bimetallic nanocatalysts, PtRu nanocatalysts exhibit a superior activity in DMFC and DEFC. Methanol and ethanol oxidation on PtRu nanocatalysts are primarily based on the balance between initial adsorptive dehydrogenation of methanol or ethanol and subsequent oxidative removal of dehydrogenation fragments [10,11]. Using methanol oxidation as an example, the first step in this reaction is the methanol adsorption. The second step is the methanol dehydrogenation and the formation of adsorbed methanolic residues (CO) on Pt surface. When pure Pt surface is occupied by the monoxide, this phenomenon is defined as surface poisoning.

$$Pt + CH_3OH \rightarrow Pt - CH_3OH_{ads} \rightarrow Pt - CO_{ads} + 4H^+ + 4e^- \quad (1)$$

The dissociation of water occurs via its reaction with the second metal Ru as represented in step 2 [12].

$$Ru + H_2O \rightarrow Ru - OH_{ads} + H^+ + e^- \quad (2)$$

The reaction of chemisorbed CO with chemisorbed hydroxyl species (OH_{ads}) has been demonstrated to remove the CO_{ads} from Pt active sites. Consequently, OH_{ads} and methanolic residues adsorbed on Pt sites can be reduced forming pure Pt and pure Ru [12].

$$Pt - CO_{ads} + Ru - OH_{ads} \rightarrow Pt + Ru + CO_2 + H^+ + e^- \quad (3)$$

The above reaction mechanism is similar for ethanol oxidation. The difference between methanol oxidation and ethanol oxidation is that the process of ethanol oxidation requires more steps and consumes more energy for C–C-bond splitting. Furthermore, adjustment of pH has been considered as a promoter to enhance the performance of DMFCs and DEFCs [13]. Zhao et al. have reported that Pd/polypyrrole–graphene operated in alkaline solution can improve MOR activity [14]. The study on the effect of the acidic solution on EOR has also been investigated [15]. Another method to promote the performance of DMFCs and DEFCs is to change atomic ratio of Pt to Ru. Shao et al. have shown that atomic ratio of Pt to Ru has a significant effect on the performance of the catalyst for methanol oxidation [16]. It also has been demonstrated that Ru has the most pronounced effect on the methanol oxidation rate when mixed with Pt in a 1:1 atomic ratio [17]. However, the pure PtRu nanocatalyst without carbon supporting materials for DMFCs and DEFCs has limitations, such as slow kinetics of the oxidation reaction and poor tolerance to CO poisoning. Carbon nanoparticles, carbon nanotubes (CNTs), and graphene are thus used as the supporting materials for PtRu nanocatalyst in the anode of a DMFC or DEFC [18].

Graphene is a two dimensional monolayer of carbon atoms which can be considered as an electrocatalyst platform due to its high specific surface area, high charge carrier mobility, chemical stability, and thermal stability [19,20]. Hybridization of graphene with metal has been investigated in different applications such as lithium batteries [21], catalysts [22], fuel cells [5], biosensors [23], and photovoltaic devices [24]. However, the large resistance from structural defects and the strong planar stacking of graphene sheets lead to a drastic deterioration of properties [3,25,26]. In order to overcome these shortcomings and extend the unique properties of graphene into the third dimension (3D), a great effort has been focused on the preparation of graphene 3D skeletons (graphene foam/porous graphene) [27,28]. Graphene foam (GF) is a 3D multilayer consisting of freestanding and monolithic graphene film. This porous architecture of 3D GF holds large surface and highly conductive pathways which is a promising material for use in energy storage and chemical sensing [29,30]. 3D GF can also be used as a freestanding electrode with a low resistance enhancing the mobility of charge carries [31].

Recently, Hu and co-workers have reported on the development of 3D GF with Pt/PdCu nanocatalyst for its application in ethanol fuel cell [3]. The results show that 3D GF can assist nanocatalysts to have better catalytic activity. In the present work, we report the preparation of novel 3D GF using Ni foam as a sacrificial template in a facile process. Furthermore, we report PtRu nanoparticles anchored onto the 3D GF as a new composite material of hierarchically structured PtRu/3D GF for anodic electrocatalysis. 3D porous graphene structure as a support for PtRu nanoparticles provided enhanced surface area for electron transfer for methanol and ethanol oxidation. PtRu/3D GF nanocatalyst exhibited catalytic activity for MOR (109.3 mA cm^{-2}) and EOR (78.6 mA cm^{-2}) which was about 2 times higher than that of PtRu/Graphene, respectively. After cyclic voltammetry (CV) for 900 cycles, the catalytic activity of PtRu/3D GF nanocatalyst also showed a higher tolerance to CO poisoning. The good conductivity of 3D GF, large active surface area of the composite material led to the enhanced catalytic activity. 3D PtRu/GF nanocatalyst provides new avenues for design of high performance electrode materials for DMFCs and DEFCs.

2. Experimental

2.1. Materials

Ruthenium (III) chloride hydrate ($RuCl_3 \cdot nH_2O$, 99.8% purity), hexachloroplatinic acid (IV) hexahydrate ($H_2PtCl_6 \cdot 6H_2O$, 37.5% Pt basis), citric acid (99.5 wt.%) and sodium borohydride ($NaBH_4$, 99 wt.%) were purchased from Sigma Aldrich (St. Louis, MO). Nafion solution (LIQUION) was purchased from Ion Power Inc (New Castle, DE). Vulcan XC-72R carbon (Cabot corporation, Boston, MA) and 12 nm flakes graphene (Graphene Supermarket, Calverton, NY) were used as received.

2.2. Growth of the 3D graphene foam

The heteroatom-free pure carbon 3D graphene foams (GFs) were grown by conventional chemical vapor deposition (CVD). Detailed procedures for preparing the 3D GFs were reported elsewhere [18]. Specifically, a nickel foam with pore size 590 μm was used and heated in Ar (500 sccm) and H_2 (200 sccm) sequentially. Graphene coated nickel foam was formed by introducing CH_4 (5 sccm). The 3D GF was then dip-coated with a poly(methyl methacrylate) (PMMA) solution (6 M in toluene) preventing structural failure of the resultant GFs. The PMMA covered GF in nickel substrate was then placed in a 3 M HCl solution removing the nickel template and dissolving the PMMA by acetone to obtain 3D GF.

2.3. Synthesis and modification of PtRu nanoparticle catalyst

Various Pt based bimetallic catalysts were studied [32], and PtRu appeared to be attractive as nanocatalyst for methanol and ethanol oxidation applications. Thus, the PtRu nanoparticles were synthesized via the borohydride reduction. The details of the preparation of PtRu nanoparticles were described elsewhere [23]. In brief, aqueous solutions of the H_2PtCl_6 (1.8 mM) and $RuCl_3$ (1.8 mM) were used as the precursors of this preparation. The quantity of $RuCl_3$ was added based on Pt to Ru atomic ratio 1:1. The prepared PtRu nanoparticles were then mixed with various carbon supporting materials: 0D active carbon particles (Vulcan XC-72R carbon), 2D commercial graphene and 3D GF. For each testing of DMFC or DEFC, the loading of Pt nanocatalyst at the electrode (surface area:

0.196 cm^2) was calculated as 0.68 $m^2\ g^{-1}$. 20 wt.% loading of PtRu nanoparticles was used in this study.

2.4. Characterization of PtRu nanocatalysts

Phase structures and compositions of the PtRu nanocatalysts with different carbon supporting materials were characterized by XRD. The crystal size was calculated using Debye–Scherrer's equation. The morphologies of the PtRu nanoparticles were examined by SEM and STEM, and details were presented elsewhere [23]. N_2 adsorption/desorption (BET) analysis was performed at 77 K using a NOVA 4200e (Quantachrome®, Boynton Beach, FL). Before the BET analysis, samples were degassed at 120 °C for 5 h.

2.5. Electrochemical characterization

CV studies of MOR and EOR were performed using an Electrochemical Workstation (CHI 660C, CH Instrument, Inc., Austin, TX). Typically, one milligram of the bimetallic nanocatalyst with the carbon based substrate was dispersed in 45 μL of ethanol and 5 μL of Nafion solution (15 wt.%), and then sonicated for 10 min to prepare the ink. After sonication, 8.0 μL of the mixture was deposited onto a glassy carbon working electrode with a surface area of 0.196 cm^2 (Part no. AFE2M050GC, PINE Instrument Company, Grove City, PA). A Pt mesh electrode (1 cm^2) and a saturated calomel electrode (SCE) were used as a counter and a reference electrode, respectively. The solutions consisted of 0.5 M H_2SO_4 + 1.0 M methanol or 1.0 M ethanol and were purged with N_2 before each experiment. Before data collection, the electrode was cleaned with 15 CV scans in the voltage range of −0.241 V to +1.2 V versus SCE at 0.1 V s^{-1}. CV studies were then conducted between −0.241 V and +1.2 V at a CV rate of 0.05 V s^{-1} for 900 cycles.

The CO stripping technique was used to determine the electrochemical active surface area (ECSA). The CO stripping voltammograms were conducted with a three electrode cell using 0.5 M H_2SO_4 as electrolyte. Pure CO (99.5%) was pre-adsorbed onto the nanocatalyst surface at −0.15 V versus SCE for 1 h. The dissolved CO was then removed by bubbling N_2 into the solution for 30 min, and the stripping voltammograms were collected at a scan rate of 0.5 V s^{-1}. Two cyclic voltammograms were recorded between −0.2 V and +1.2 V versus SCE. The first potential sweep was conducted to electro-oxidize the adsorbed CO and the second potential sweep was to verify the completeness of the CO oxidation.

3. Results and discussion

3.1. Physicochemical characterization of PtRu nanocatalysts with different carbon supporting materials

3D GF revealed a macroporous structure with a pore diameter of 50–250 μm and extremely thin interconnected sheets of graphene providing sufficient binding sites for PtRu nanoparticles, as shown in Fig. 1(a). The STEM image of Fig. 1(b) showed PtRu nanoparticles covering the entire surface of the 3D GF nanoporous structure uniformly. Details of this assessment were reported elsewhere [23]. The crystal size of each sample also could be verified by the XRD results.

XRD patterns of PtRu nanoparticles with different carbon supporting materials were reported [23]. The diffraction patterns from the (111), (200), (220) and (311) planes of the Pt crystal were given. The crystal sizes of the PtRu, PtRu/C, PtRu/Graphene were 7.07, 5.39 and 4.24 nm, respectively. In summary, the PtRu/3D GF nanocatalyst showed the smallest crystal size of 3.51 nm, indicating it had the largest surface area per unit volume among the four nanocatalysts. Consequently, the PtRu/3D GF nanocatalyst would be attractive to catalyze the methanol or ethanol oxidation reactions.

3.2. Surface area measurements

CO stripping voltammetry is a reliable method applied to evaluate the ECSA of the nanocatalyst [33,34]. The ECSA is calculated by

$$\mathrm{ECSA} = \frac{Q_{co}}{[\mathrm{Pt}] \times 420\ \mu\mathrm{C\ cm^{-2}}} \tag{4}$$

where Q_{co} is the charge for the CO stripping (mC cm^{-2}), [Pt] is the platinum loading (mg cm^{-2}) in the electrode, and 420 μC cm^{-2} represents the charge density which is required to oxidize a monolayer of CO on the Pt site. In this study, the ECSA values were 37.2 $m^2\ g^{-1}$, 54.2 $m^2\ g^{-1}$, 121.8 $m^2\ g^{-1}$ and 186.2 $m^2\ g^{-1}$ for the PtRu, PtRu/C, PtRu/Graphene and PtRu/3D GF, respectively. The PtRu/3D GF nanocatalyst showed higher ECSA compared to the other three nanocatalysts. This observation was in agreement with the experimental results stated by XRD that PtRu/3D GF nanocatalyst had the largest surface area based on crystal size.

BET was used to measure the total specific surface area by evaluating the external area and the pore area of a material. This technique is based on physical adsorption of a monolayer of gas

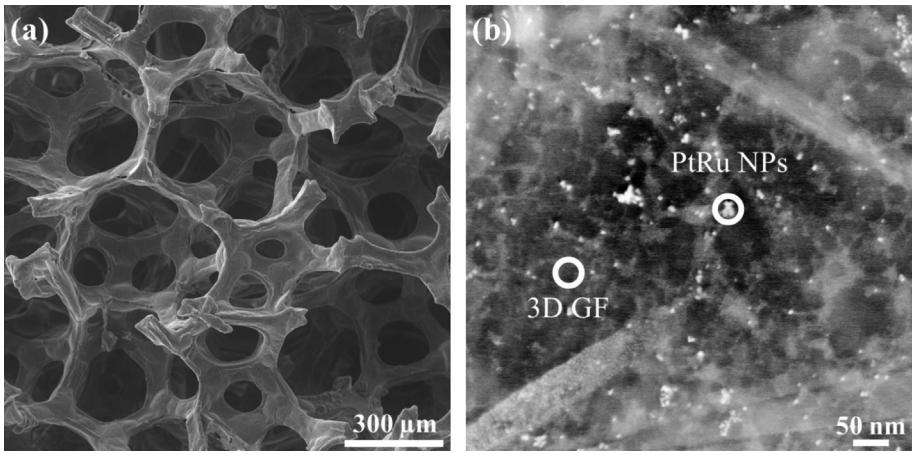

Fig. 1. (a) SEM image of pure graphene foam, (b) STEM image of PtRu/3D GF.

molecules on the surface of a material. The data are then treated according to the Brunauer, Emmett and Teller adsorption isotherm equation [35]. In this study, the BET surface area values of the PtRu, PtRu/C, PtRu/Graphene and PtRu/3D GF were measured by N_2 adsorption/desorption and were 44.9 $m^2\ g^{-1}$, 52.9 $m^2\ g^{-1}$, 135.7 $m^2\ g^{-1}$ and 158.6 $m^2\ g^{-1}$, respectively. PtRu/3D GF was more than triple that of the commercial carbon support, Vulcan XC-72R carbon powder. It was expected that not all of the surface area of the nanocatalysts for processes of electro-oxidation could be measured by BET due to the fineness of the porosity defined by such small nanoparticle size. However, the trend of CO stripping voltammetry was consistent with the trend of BET measurement.

3.3. Methanol and ethanol oxidation measurements

Fig. 2(a) and (b) shows the cyclic voltammograms for methanol and ethanol oxidation in a solution of 0.5 M H_2SO_4 + 1 M CH_3OH and 0.5 M H_2SO_4 + 1 M C_2H_5OH over PtRu nanocatalysts with different carbon supporting materials, respectively. The potential was swept between −0.2 and +1.2 V versus saturated calomel electrode (SCE) at a voltage scan rate of 0.05 V s^{-1}. For the methanol and ethanol oxidation, PtRu catalysts with different carbon supporting materials showed similar trends. The addition of methanol or ethanol to the electrolyte resulted in a dramatic change in the appearance of voltammograms due to MOR or EOR taking place on the surface of the nanocatalysts as shown in Fig. 2(a) and (b). Methanol and ethanol oxidation were characterized by well-separated anodic peaks in the forward (I_f) and reverse (I_b) scans. The magnitude of peak in forward scan was directly proportional to the amount of methanol or ethanol oxidized at the nanocatalyst electrode. The reverse scan was attributed to the removal of carbon monoxide (CO) and other residual carbonaceous species formed in the forward scan. PtRu/3D GF showed the highest current density (I_f) of oxidation reaction for both methanol (109.3 mA cm^{-2}) and ethanol (78.6 mA cm^{-2}) compared to the other carbon supporting materials. The current density (I_f) of the PtRu/3D GF was 4.35 and 2.13 times higher than that of PtRu/C and PtRu/Graphene for MOR, respectively. In EOR, the current density (I_f) of the PtRu/3D GF was 2.32 and 1.86 times higher than that of PtRu/C and PtRu/Graphene, respectively. The increased number of active adsorption sites and the larger surface area accelerated the reaction rate resulting in the enhanced catalytic activity.

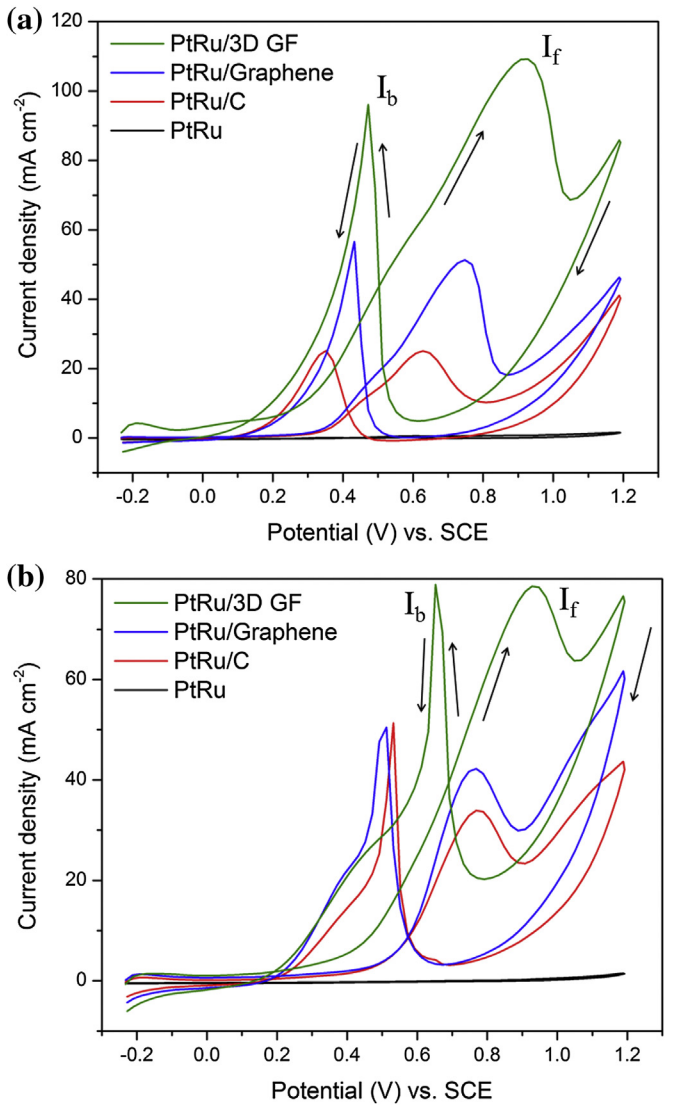

Fig. 2. The cyclic voltammograms of PtRu nanocatalysts with different carbon supporting materials (a) in a solution of 0.5 M H_2SO_4 and 1 M CH_3OH, (b) in a solution of 0.5 M H_2SO_4 and 1 M C_2H_5OH.

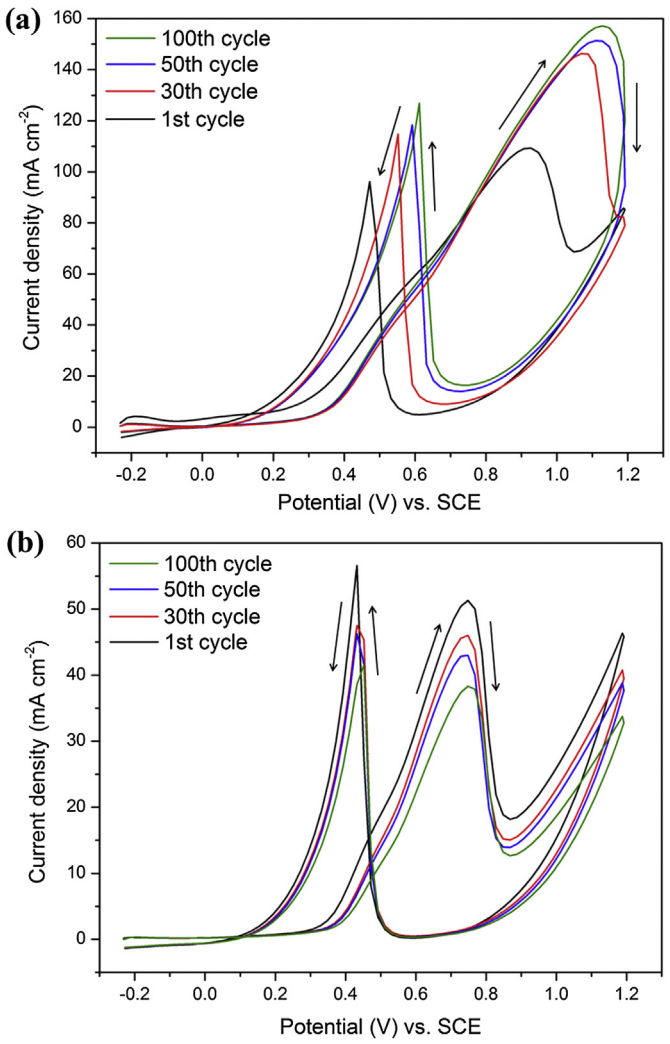

Fig. 3. The cyclic voltammograms of two PtRu nanocatalysts for 100 cycles in a solution of 0.5 M H_2SO_4 and 1 M CH_3OH (a) PtRu/3D GF, (b) PtRu/Graphene.

The resistance to CO poisoning was also an important concern for nanocatalysts. The ratio of peak currents associated with the anodic peaks in forward (I_f) and reverse (I_b) was used to describe the tolerance of a catalyst to intermediates generated during the oxidation of methanol [12]. A low I_f/I_b ratio indicated poor electro-oxidation of methanol to CO during the forward scan, suggesting excessive accumulation of carbonaceous intermediates on the catalyst surface [36]. For PtRu/3D GF nanocatalyst, the value of I_f/I_b was 1.14 which was larger than that of PtRu/C (0.99) and PtRu/Graphene (0.91) for MOR. In EOR, the I_f/I_b value of PtRu/3D GF nanocatalyst was 1.00 which was also larger than that of PtRu/C (0.66) and PtRu/Graphene (0.84). This result suggested that PtRu/3D GF nanocatalyst possessed a relatively higher tolerance to CO poisoning and the carbonaceous intermediates. The onset potential of the methanol and ethanol oxidation reaction for the PtRu/3D GF were shifted towards more negative potentials than the PtRu/C and PtRu/Graphene. Thus, the reduction in the overpotential for PtRu/3D GF suggested that PtRu/3D GF nanocatalyst could be used to lower the kinetic resistance to dissociate methanol or ethanol.

The catalytic activity and stability of the PtRu/3D GF nanocatalyst were also demonstrated in Fig. 3 for MOR and Fig. 4 for EOR in comparison with PtRu/Graphene nanocatalyst, respectively. The cyclic voltammograms of PtRu/3D GF and PtRu/Graphene nanocatalysts in a solution of 0.5 M H_2SO_4 and 1 M CH_3OH at a voltage scan rate of 0.05 V s^{-1} for 100 cycles were shown in Fig. 3. For PtRu/3D GF nanocatalyst, the current density of the first scan at both forward and reverse scan peaks increased from 109.3 and 96.2 mA cm^{-2} to 146.2 and 114.8 mA cm^{-2} in the 30 cycles, and then continuously increased to 151.3 mA cm^{-2} and 118.4 mA cm^{-2} in the 50th cycle, respectively. In 100th cycle, the current density at both forward and reverse scan peaks were enhanced to 157.2 and 126.9 mA cm^{-2}, as shown in Fig. 3(a). For PtRu/Graphene nanocatalyst, a decrease in current density at both forward and reverse scan peaks were observed in 30 cycles. After 30 cycles, the current density at both forward and reverse scan peaks gradually decreased from 46.0 and 45.3 mA cm^{-2} in the 30th cycle to 38.3 and 41.5 mA cm^{-2} in the 100th cycle, as shown in Fig. 3(b). The cyclic voltammograms of PtRu/3D GF and PtRu/Graphene nanocatalysts in a solution of 0.5 M H_2SO_4 and 1 M C_2H_5OH at a voltage scan rate of 0.05 V s^{-1} for 100 cycles were shown in Fig. 4. For PtRu/3D GF nanocatalyst (Fig. 4(a)), the current density in the first forward scan decreased from 78.6 mA cm^{-2} to 58.5 mA cm^{-2} in the 30th cycle, and then continuously decreased to 54.8 mA cm^{-2} and

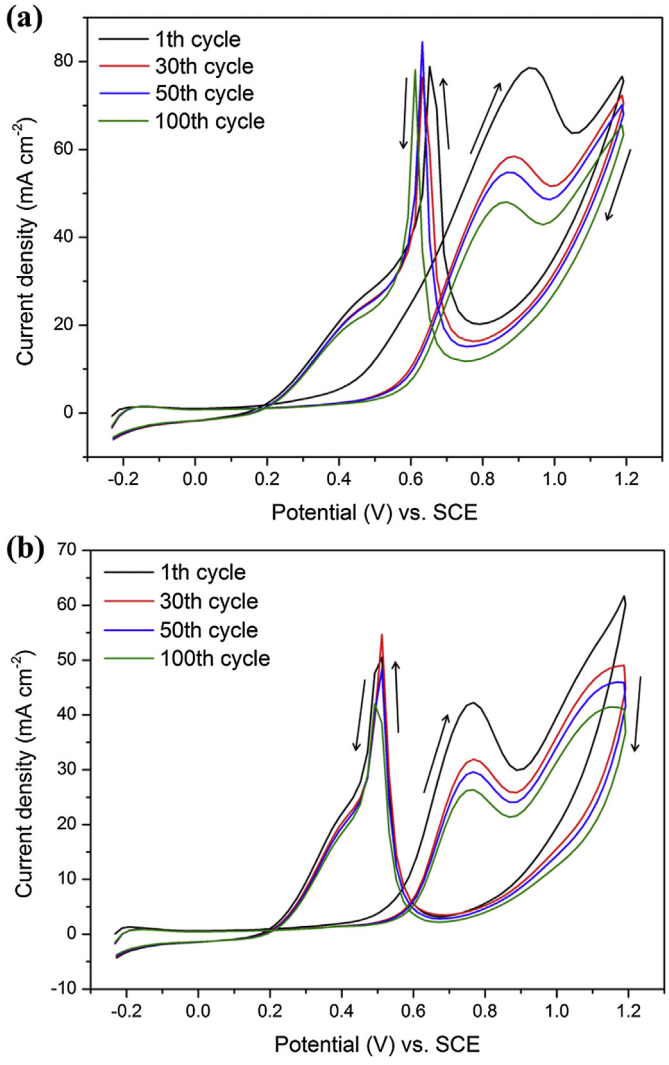

Fig. 4. The cyclic voltammograms of two PtRu nanocatalysts for 100 cycles in a solution of 0.5 M H_2SO_4 and 1 M C_2H_5OH (a) PtRu/3D GF, (b) PtRu/Graphene.

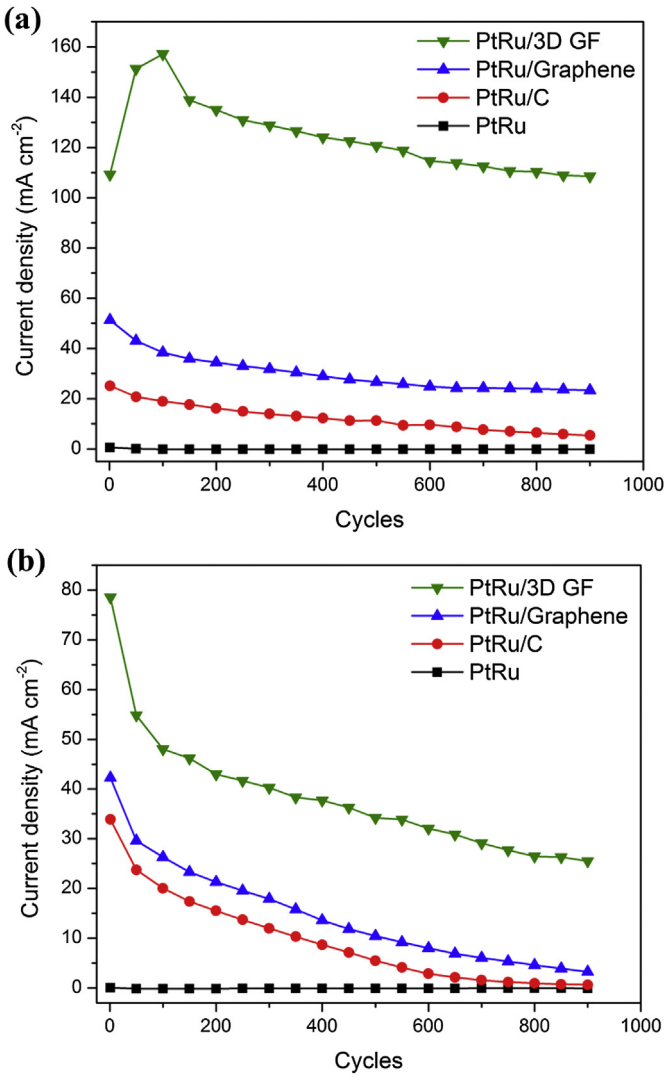

Fig. 5. The durability performance of PtRu nanocatalysts with different carbon supporting materials (a) for methanol oxidation reaction, (b) for ethanol oxidation reaction.

Table 1
A comparison of the performance of the PtRu/3D GF, PtRu/Graphene and PtRu/C nanocatalysts for methanol and ethanol oxidation reactions.

Catalyst	Crystal size (nm)	ECSA ($m^2\ g^{-1}$)	BET ($m^2\ g^{-1}$)	Methanol oxidation			Ethanol oxidation		
				I_f (mA cm^{-2})	I_f/I_b ratio	I_f at the 900th cycle (mA cm^{-2})	I_f (mA cm^{-2})	I_f/I_b ratio	I_f at the 900th cycle (mA cm^{-2})
PtRu/3D GF	3.51	186.2	158.6	109.3	1.14	108.5	78.6	1.00	25.5
PtRu/Graphene	4.24	121.8	135.7	51.3	0.91	23.3	42.3	0.84	3.3
PtRu/C	5.39	54.2	52.9	25.1	0.99	5.3	33.9	0.66	0.6

48.0 mA cm^{-2} in the 50th and 100th cycle, respectively. For PtRu/Graphene nanocatalyst (Fig. 4(b)), a decrease in current density at forward scan peak was observed, following by 42.3 mA cm^{-2} in the 1st cycle, 31.9 mA cm^{-2} in the 30th cycle, 29.6 mA cm^{-2} in the 50th cycle, and 26.3 mA cm^{-2} in the 100th cycle. Both the anodic peaks in forward scan (I_f) in MOR (Fig. 3) and EOR (Fig. 4) shifted towards positive potential as the cycle's number increased. This higher potential of MOR and EOR suggested that the Pt surface was poisoned by CO continuously and nanocatalyst itself therefore had to overcome the higher overpotential to dissociate of methanol or ethanol. It was clear that 3D GF used as the supporting materials exhibited a higher and more stable catalytic activity than commercial graphene and vulcan XC-72R carbon in MOR and EOR. Hu and Zhang state that the agglomeration of nanoparticles appears after potential cycling which is due to the Ostwald ripening process [3,5]. However, PtRu nanoparticles on 3D GF have the finer dispersion and stronger attachment than on Vulcan XC-72R carbon and commercial graphene keeping itself from agglomeration and Ostwald ripening. PtRu nanoparticles with relatively uniform dispersions on 3D GF would reduce and prevent the agglomeration phenomenon and therefore maintain the superior catalytic activity and stability during the potential cycling.

In order to investigate the long-term cycle stability of the nanocatalysts, CV measurements were performed for 900 cycles. Fig. 5(a) and (b) showed the durability performance of PtRu nanocatalyst with different carbon supporting materials for MOR and EOR, respectively. The current density for both MOR and EOR showed a rapid decay in the initial period for PtRu/C and PtRu/Graphene nanocatalysts. The result showed that after 900 cycles the current density of PtRu/C, PtRu/Graphene, PtRu/3D GF nanocatalysts were reduced by 78.8%, 54.6%, and 0.7% of their initial current density for MOR and decreased by 98.1%, 92.3%, and 67.5% of their initial current density for EOR, respectively. The current density of PtRu/3D GF nanocatalyst remained around 110 mA cm^{-2} after 900 cycles for MOR which was 20.5 and 4.7 times higher than PtRu/C and PtRu/Graphene, respectively. In EOR, the current density of PtRu/3D GF nanocatalyst was around 25 mA cm^{-2} after 900 cycles which was 40.5 and 7.7 times higher than PtRu/C and PtRu/Graphene, respectively. All physical and electrochemical characteristics of PtRu bimetallic catalysts on the various carbon supports are summarized in Table 1. PtRu/3D GF nanocatalyst showed superior performance compared to the other catalysts studied, which is due to the large surface area and high catalytic activity of PtRu/3D GF. Figs. 2 to 5 illustrate the details of the oxidation reactions of methanol and ethanol, the profiles of the MOR and EOR were similar, but the magnitudes of current density were different.

4. Conclusions

In summary, a new nanocatalyst system of PtRu bimetallic nanoparticles decorated on 3D GF was fabricated. Anchoring bimetallic nanocatalysts onto 3D porous structure enhanced the active surface area and increased the effective transport of the reactants. The MOR and EOR activities of PtRu/3D GF were not only better than those of PtRu and PtRu/C, but also showed substantial improvement over PtRu/Graphene after prolonged cycling. 3D GF provided the uniform distribution of PtRu nanoparticles, improved the availability ECSA of nanocatalyst for electron transfer, and enhanced the tolerance to CO poisoning. The PtRu/3D GF nanocatalyst thus enhanced the rates of methanol and ethanol oxidation reactions.

Acknowledgments

This study was supported by the DOD-Air Force Office of Scientific Research-MURI 2011-microfabrication. Technical assistance from the staff of Electronics Design Center of Case Western Reserve University is gratefully acknowledged.

References

[1] L. Dai, D.W. Chang, J.B. Baek, W. Lu, Small 8 (2012) 1130–1166.
[2] H.J. Choi, S.M. Jung, J.M. Seo, D.W. Chang, L. Dai, J.B. Baek, Nano Energy 1 (2012) 534–551.
[3] C. Hu, H. Cheng, Y. Zhao, Y. Hu, Y. Liu, L. Dai, L. Qu, Adv. Mater. 24 (2012) 5493–5498.
[4] H.P. Cong, X.C. Ren, S.H. Yu, ChemCatChem 4 (2012) 1555–1559.
[5] Y. Zhang, M. Janyasupab, C.W. Liu, X. Li, J. Xu, C.C. Liu, Adv. Funct. Mater. 22 (2012) 3570–3575.
[6] S. Chakraborty, C.R. Raj, Biosens. Bioelectron. 24 (2009) 3264–3268.
[7] S. Şen, F. Şen, G. Gökağaç, Phys. Chem. Chem. Phys. 13 (2011) 6784–6792.
[8] S. Alayoglu, A.U. Nilekar, M. Mavrikakis, B. Eichhorn, Nat. Mater. 7 (2008) 333–338.
[9] S.Y. Huang, C.M. Chang, K.W. Wang, C.T. Yeh, Chem. Phys. Chem. 8 (2007) 1774–1777.
[10] H.A. Gasteiger, N. Markovic, P.N. Ross, E.J. Cairns, J. Phys. Chem. 97 (1993) 12020–12029.
[11] P. Kauranen, E. Skou, J. Munk, J. Electroanal. Chem. 404 (1996) 1–13.
[12] M. Watanabe, S. Motoo, J. Electroanal. Chem. 60 (1975) 275–283.
[13] V.R. Gangwal, J.V.D. Schaaf, B.F.M. Kuster, J.C. Schoutem, J. Catal. 229 (2005) 389–403.
[14] Y. Zhao, L. Zhan, J. Tian, S. Nie, Z. Ning, Electrochim. Acta 56 (2011) 1967–1972.
[15] Z.B. Wang, P.J. Zuo, G.J. Wang, C.Y. Du, G.P. Yin, J. Phys. Chem. C 112 (2008) 6582–6587.
[16] Z.G. Shao, F. Zhu, W.F. Lin, P.A. Christensen, H. Zhang, J. Power Sources 161 (2006) 813–819.
[17] A.J. Dickinson, L.P.L. Carrette, J.A. Collins, K.A. Friedrich, U. Stimming, J. Appl. Electrochem. 34 (2004) 975–980.
[18] J. Prabhuram, T.S. Zhao, Z.K. Tang, R. Chen, Z.X. Liang, J. Phys. Chem. B 110 (2006) 5245–5252.
[19] R.S. Sundaram, M. Steiner, H.Y. Chiu, M. Engel, A.A. Bol, R. Krupke, M. Burghard, K. Kern, P. Avouris, Nano Lett. 11 (2011) 3833–3837.
[20] H. Wang, Y. Yang, Y. Liang, J.T. Robinson, Y. Li, A. Jackson, Y. Cui, H. Dai, Nano Lett. 11 (2011) 2644–2647.
[21] Z.S. Wu, W. Ren, L. Wen, L. Gao, J. Zhao, Z. Chen, G. Zhou, F. Li, H.M. Cheng, ACS Nano 4 (2010) 3187–3194.
[22] G.M. Scheuermann, L. Rumi, P. Steurer, W. Bannwarth, R. Mulhaupt, J. Am. Chem. Soc. 131 (2009) 8262–8270.
[23] C.C. Kung, P.Y. Lin, F.J. Buse, Y. Xue, X. Yu, L. Dai, C.C. Liu, Biosens. Bioelectron. 52 (2014) 1–7.
[24] S. Guo, S. Dong, E. Wang, ACS Nano 4 (2010) 547–555.
[25] H. Bi, F. Huang, J. Liang, Y. Tang, X. Lü, X. Xie, M. Jiang, J. Mater. Chem. 21 (2011) 17366–17370.
[26] Z. Chen, W. Ren, L. Gao, B. Liu, S. Pei, H.M. Cheng, Nat. Mater. 10 (2011) 424–428.
[27] S.H. Lee, H.W. Kim, J.O. Hwang, W.J. Lee, J. Kwon, C.W. Bielawski, R.S. Ruoff, S.O. Kim, Angew. Chem. Int. Ed. 49 (2010) 10084–10088.
[28] S. Yin, Y. Zhang, J. Kong, C. Zou, C.M. Li, X. Lu, J. Ma, F.Y.C. Boey, X. Chen, ACS Nano 5 (2011) 3831–3838.

[29] X. Huang, K. Qian, J. Yang, J. Zhang, L. Li, C. Yu, D. Zhao, Adv. Mater. 24 (2012) 4419–4423.
[30] E. Singh, Z. Chen, F. Houshmand, W. Ren, Y. Peles, H.M. Cheng, N. Koratkar, Small 1 (2013) 75–80.
[31] P. Si, X.C. Dong, P. Chen, D.H. Kim, J. Mater. Chem. B 1 (2013) 110–115.
[32] Y. Zhang, M. Janyasupab, C.W. Liu, P.Y. Lin, K.W. Wang, J. Xu, C.C. Liu, Int. J. Electrochem. (2012), http://dx.doi.org/10.1155/2012/410846.
[33] M.S. Saha, R. Li, X. Sun, Electrochem. Commun. 9 (2007) 2229–2234.
[34] R. Chetty, S. Kundu, W. Xia, M. Bron, W. Schuhmann, V. Chirila, W. Brandle, T. Reinecke, M. Muhler, Electrochim. Acta 54 (2009) 4208–4215.
[35] S. Brunauer, P.H. Emmett, E. Teller, J. Am. Chem. Soc. 60 (1938) 309–319.
[36] C.W. Liu, Y.W. Chang, Y.C. Wei, K.W. Wang, Electrochim. Acta 56 (2011) 2574–2581.